Nonlinear optical imaging and spectral-lifetime computational analysis of endogenous and exogenous fluorophores in breast cancer

Paolo P. Provenzano
University of Wisconsin
Departments of Pharmacology and Biomedical Engineering
    and
Laboratory for Optical and Computational Instrumentation
    and
Paul P. Carbone Comprehensive Cancer Center
Madison, Wisconsin 53706

Curtis T. Rueden
University of Wisconsin
Laboratory for Optical and Computational Instrumentation
Madison, Wisconsin 53706

Steve M. Trier
University of Wisconsin
Department of Biomedical Engineering
    and
Laboratory for Optical and Computational Instrumentation
    and
Paul P. Carbone Comprehensive Cancer Center
Madison, Wisconsin 53706

Long Yan
University of Wisconsin
Department of Biomedical Engineering
    and
Laboratory for Optical and Computational Instrumentation
Madison, Wisconsin 53706

Suzanne M. Ponik
University of Wisconsin
Departments of Pharmacology and Biomedical Engineering
    and
Laboratory for Optical and Computational Instrumentation
    and
Paul P. Carbone Comprehensive Cancer Center
Madison, Wisconsin 53706

David R. Inman
University of Wisconsin
Department of Pharmacology
    and
Paul P. Carbone Comprehensive Cancer Center
Madison, Wisconsin 53706

Patricia J. Keely
University of Wisconsin
Departments of Pharmacology and Biomedical Engineering
    and
Laboratory for Optical and Computational Instrumentation
    and
Paul P. Carbone Comprehensive Cancer Center
Madison, Wisconsin 53706

Kevin W. Eliceiri
University of Wisconsin
Department of Biomedical Engineering
    and
Laboratory for Optical and Computational Instrumentation
Madison, Wisconsin 53706

Abstract. Multiphoton laser scanning microscopy (MPLSM) utilizing techniques such as multiphoton excitation (MPE), second harmonic generation (SHG), and multiphoton fluorescence lifetime imaging and spectral lifetime imaging (FLIM and SLIM, respectively) are greatly expanding the degree of information obtainable with optical imaging in biomedical research. The application of these nonlinear optical approaches to the study of breast cancer holds particular promise. These noninvasive, multidimensional techniques are well suited to image exogenous fluorophores that allow relevant questions regarding protein localization and signaling to be addressed both *in vivo* and *in vitro*. Furthermore, MPLSM imaging of endogenous signals from collagen and fluorophores such as nicotinamide adenine dinucleotide (NADH) or flavin adenine dinucleotide (FAD), address important questions regarding the tumor-stromal interaction and the physiologic state of the cell. We demonstrate the utility of multimodal MPE/SHG/FLIM for imaging both exogenous and/or endogenous fluorophores in mammary tumors or relevant 3-D systems. Using SLIM, we present a method for imaging and differentiating signals from multiple fluorophores that can have overlapping spectra via SLIM Plotter—a computational tool for visualizing and analyzing large spectral-lifetime data sets. © *2008 Society of Photo-Optical Instrumentation Engineers.* [DOI: 10.1117/1.2940365]

Keywords: endogenous fluorescence; multiphoton microscopy; second harmonic generation; fluorescence lifetime imaging microscopy; spectral lifetime imaging microscopy.

Paper 07341SSR received Nov. 14, 2007; revised manuscript received Nov. 18, 2008; accepted for publication Nov. 18, 2008; published online Jul. 2, 2008.

1 Introduction

Breast cancer is a devastating disease accounting for ~15% of all female cancer-related deaths in the United States and is

Address all correspondence to Kevin Eliceiri, Laboratory for Optical and Computational Instrumentation, University of Wisconsin at Madison, 271 Animal Sciences, 1675 Observatory Drive, Madison, WI 53706; Tel: 608–263–6288; Fax 608–262–4570; E-mail: eliceiri@wisc.edu

the most prevalent cancer among women.[1] Therefore, technologies to detect, classify, study, and combat breast cancer are of great significance. Among these technologies, optical imaging modalities have helped facilitate advances in cancer diagnosis as well as aid in studies aimed at understanding the mechanisms associated with cancer formation and progression (reviewed in Refs. [2] and [3]). Often, relevant questions regarding complex cell signaling events and physiological processes can only be well understood by imaging temporal molecular localization events and other subcellular processes in cells in their engineered or native environment. As such, nonlinear optical imaging techniques based on multiphoton excitation have emerged as powerful tools to noninvasively image cellular processes both *in vitro* and *in vivo*.[4–11]

Multiphoton laser scanning microscopy (MPLSM), first reported by Denk and colleagues,[8] is an optical sectioning technique that allows thick biological sections to be imaged via absorption of two or more low-energy photons (typically 700 to 1050 nm). For this reason, the effective imaging depth can greatly exceed conventional confocal microscopy,[8,12] while reducing photo damage and maintaining superior viability following prolonged exposure.[13] As a result of these characteristics, the use of multiphoton imaging technology is increasing, which has facilitated the emergence of two-photon second harmonic generation (SHG) imaging of biological structures,[5–7,10,14] multiphoton fluorescence lifetime imaging microscopy (FLIM; Refs. [15–18]), and multiphoton spectral lifetime imaging microscopy (SLIM; Refs. [19] and [20]). Hence, when utilized individually, and particularly in combination, these advances provide tools to obtain detailed multidimensional data from cells containing exogenous and/or endogenous fluorophores.

Engineering of proteins tagged with exogenous fluorophores, such as Green Fluorescent Protein (GFP) and DsRed (and their variants), has greatly expanded our knowledge of fundamental intracellular processes affording unparalleled insight into protein localization, interactions, and temporal dynamics (reviewed in Refs. [21–23]). In particular, recent advances using exogenous fluorophores to generate (fluorescence resonance energy transfer (FRET)) are providing new information about complex signaling events within cancerous cells.[24,25] However, imaging complex systems and multiple fluorophores presents certain obstacles. One such difficulty arises from overlapping spectra and background signals from endogenous fluorophores. Yet endogenous fluorophores can also provide useful structural information about the interaction of a cell with its microenvironment[14,26–28] and the condition of the cell.[29–32] For instance: (1) endogenous SHG signals from collagen have provided fundamental information regarding the tumor cell's interaction with the stroma during invasion and metastasis,[14,26] (2) the metabolic state of carcinoma cells, as detected by endogenous fluorophores that are metabolic intermediates, has been correlated to metastatic potential,[32] and (3) diagnosis of human cancer by examining endogenous fluorophores has been an active area of research for many years (see Refs. [32–35] and references therein). Therefore, imaging endogenous fluorophores in breast cancer tissue can provide biologically meaningful information, and the ability to account for endogenous fluorescence when imaging exogenous or combined exogenous/endogenous fluorophores is very practical.

In breast tissue, the most dominant endogenous fluorophores imaged with MPLSM are tryptophan, nicotinamide adenine dinucleotide (NADH) and flavin adenine dinucleotide (FAD), as well as endogenous SHG signals from collagen. Each of these fluorophores has a unique excitation/emission spectra in the UV and visible light regimes that allows imaging of cellular morphology and organelles (such as mitochondria), as well as providing information about the metabolic state of the cell. The excitation/emission maxima of these fluorophores are $\sim 280/340$ nm for tryptophan, $\sim 340/450$ nm for NADH, and $\sim 450/530$ nm for FAD[30,31]; two-photon SHG from collagen is a nonfluorescent event resulting from the laser field suffering a nonlinear, second-order polarization when passing through a noncentrosymmetric ordered structure, and as such, SHG signals are at exactly half the excitation wavelength.[5,36–38] Although the spectra of these strong endogenous signals are reasonably distinct, there is overlap and they are not distinct from the exogenous fluorophores most commonly utilized with MPLSM. Therefore, in order to distinguish emission signals or correct for background contamination, filtering techniques may be employed to isolate portions of the emission spectra. However, this requires an *a priori* knowledge of the fluorophores that may not always be practical. Another approach is to utilize multiphoton FLIM, where the excited state lifetimes of the fluorophores are analyzed to potentially identify fluorophores with significantly overlapping spectra. However, the excited state lifetime of a molecule is microenvironment dependent, with factors such as pH, oxygen concentration, temperature, binding to macromolecules, and FRET states all potentially modifying the lifetime of a particular fluorophore.[39] Therefore, it is desirable to obtain spectral information combined with fluorescence lifetime data to facilitate imaging of multiple fluorophores within a cell or tissue. To achieve this goal, our research group has developed a combined multiphoton spectral and lifetime microscope[19,40] for SLIM that simultaneously collects fluorescence lifetime data from 16 separate 10-nm-width spectral channels. Using this system, we are able to collect data from spectrally overlapping fluorophores and isolate signals of interest from contaminating signals. In this paper, we will present data demonstrating the utility of MPLSM-based technologies to image endogenous signals and the combination of exogenous and endogenous signals with particular emphasis on spectral lifetime imaging, and the computational tools we have developed to visualize and analyze complex spectral lifetime data sets.

2 Methods

2.1 *Cell Culture*

T47D cells were obtained from the American Type Culture Collection. NMuMG cells were a kind gift from Dr. Caroline Alexander (University of Wisconsin). EGFP-Vinculin was a kind gift from Dr. Anna Huttenlocher (University of Wisconsin). For GFP-RBD, the Rho binding domain (RBD) of Rhotetkin was excised from GFP-RBD (a generous gift of Dr. Bill Bement, University of Wisconsin), subcloned into pEGFP-C1 (Clontech), and stably expressed in T47D breast carcinoma cells. T47D human breast cells were maintained in RPMI

supplemented with 10% fetal bovine serum and insulin. NMuMG mouse mammary cells were maintained in DMEM supplemented with insulin and 10% fetal bovine serum. Both cells lines were cultured at 37°C with 5% CO_2.

Cells were cultured and imaged under standard 2-D conditions or within 3-D collagen matrices. For 3-D culture, cells were cultured within a 1.0 to 4.0 mg/mL type-I collagen gel (rat-tail collagen solution, BD Biosciences) neutralized with 100 mM HEPES in 2× PBS. Following gel polymerization, gels were soaked in cell-specific media (described earlier) or serum-free media containing BSA and maintained at 37°C with 10% CO_2 until imaged as described in the text.

2.2 Mammary Tumors

All animal experiments were approved by the institutional animal use and care committee and meet NIH guidelines for animal welfare. To generate mammary tumors, polyoma middle-T mice[41] were employed. For MPLSM imaging of live, unfixed, intact (not sectioned), nonstained PyVT tumors, tumors were harvested and live tissue maintained in buffered media at 37°C. All tissues were imaged immediately following tissue harvest.

2.3 Instrumentation

For all imaging, two different custom multiphoton systems that are part of the University of Wisconsin Laboratory for Optical and Computational Instrumentation (LOCI, www.loci.wisc.edu) were utilized.[19,40,42] The first system is an MPLSM workstation constructed around a Nikon Eclipse TE300 that facilitates multiphoton excitation (MPE), SHG, and FLIM. All SHG imaging was performed on this microscope and was detected from the backscattered SHG signal.[38] A 5-W mode-locked Ti:Sapphire laser (Spectra-Physics-Millennium/Tsunami) excitation (laser field) source producing around 100-fs pulse widths was tuned to 780 to 900 nm. The beam was focused onto the sample with a Nikon CFI Plan Fluor 20× multi-immersion objective (NA of 0.75 and WD of 0.33 with water), a Nikon CFI Plan Fluor 40× oil immersion lens (NA=1.3), or a Nikon CFI Plan Apo 60× water-immersion lens (NA=1.2). Endogenous fluorescence and SHG signals were isolated with 464-nm (cut-on) long-pass and 445-nm narrow bandpass filters, while GFP signals were isolated with a 480 to 550 nm (bandpass) filter (all filters: TFI Technologies, Greenfield, Massachusetts). Intensity and FLIM data were collected by a H7422 GaAsP photon counting photomultiplier tube (PMT) (Hamamatsu) connected to a time-correlated single photon counting (TCSPC) system (SPC-730, Becker & Hickl).

The second microscope has been recently described in detail[19,29,40] and allows generation of multiphoton excitation intensity images in conjunction with FLIM and SLIM. In short, the system is built around an inverted microscope (TE 2000, Nikon, Melville, New York) with source illumination from a Ti:Sapphire mode-locking laser (Coherent Mira, Coherent, Santa Clara, California), with a tuning range of ~700 to 1000 nm. FLIM images were acquired with an electronic system for recording fast light signals by time-correlated single photon counting (SPC-830, Becker & Hickl). The system has several detectors, including a 16-channel combined spectral lifetime detector (utilizes a Hamamatsu PML-16 PMT), detection range 350 to 720 nm, and an H7422P GaAsP photon counting PMT (Hamamatsu) for intensity and lifetime imaging. The same lenses and filters were used as on the first microscope system. Both FLIM and SLIM data were collected over 60 s, and the pixel frame size for the MPE/SHG images is 1024×1024, while the FLIM and SLIM images are 256×256.

Acquisition for both MPLSM systems was performed with WiscScan,[43] a LOCI-developed software acquisition package that can control both the MPLSM and the lifetime collection. Image analysis was performed with ImageJ[44] and VisBio[45] software. Fluorescent lifetime analysis was carried out with SPCImage (Becker & Hickl), which can fit fluorescent decay data to an exponential function [Eq. (1)], for one, two, or three terms, and sum individual photon counts for each pixel to construct a contrast image. The incomplete model approach in SPCImage was used to compensate for instances where the fluorescence decay is slow compared to the time window defined by the repetition rate of the laser system. SLIM analysis was performed with SPCImage (Becker & Hickl) and SLIM Plotter (described in detail in Sec. 3).

3 Results and Discussion

3.1 Nonlinear Optical Imaging: MPE, SHG, FLIM, and SLIM

Increased understanding of tumor-stromal interactions is a critical aspect of the study of breast tumor formation and progression, since stromal-epithelial interactions play a critical role in both tumorigenesis and metastasis.[14,26,46–49] Since optical imaging modalities allow deep, noninvasive imaging of epithelial and stromal components of live breast tissue and tumors, they provide a valuable set of tools to better understand the tumor-stromal interaction. As seen in Fig. 1, multimodal multiphoton excitation (MPE)/SHG imaging offers a clear view of intact live mammary tumor tissue. Not only can epithelial and stromal cells be clearly seen, but their interaction with the stromal collagen matrix can also be readily imaged. By taking advantage of the fact that SHG signals are exactly half of the excitation wavelength, while fluorophores under MPE excitation obey the fundamental physical relationship of energy loss after excitation (Stokes shift), the MPE and SHG signals can be separated by filtering the emission signal. In Fig. 1, live mammary tumor tissue was excited at 890 nm to produce endogenous fluorescence from tumor and tumor-associated cells and SHG from collagen. (In our hands, with our biological systems, this wavelength has provided the strongest SHG signal for collagen.) To separate the emission signals, a 464-nm (cut-on) long-pass filter was used to isolate the cellular fluorescence (MPE signal), while SHG was isolated with a 445-nm narrow bandpass filter. By performing this filtering scheme, the tumor cell's interaction with collagen can be studied. Consequently, the use of combined MPE/SHG has the ability to identify and differentiate features that are either not obtainable or not easily obtained with more traditional fluorescence microscopy techniques. For instance, using this approach, we previously defined three tumor-associated collagen signatures (TACS; Ref. 14) in mammary tumors by imaging stromal collagen density and organization within and around tumors of varying stages. These TACS are diagnostic, allowing identification of early neoplastic regions
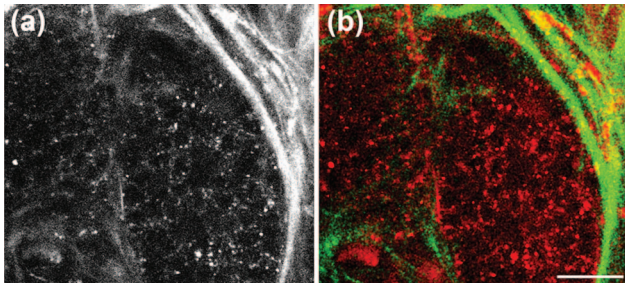
Fig. 1 MPE/SHG imaging of live tumor tissue. Combined (a) and separated (b) MPE/SHG images acquired following $\lambda_{ex}=890$ nm of live mammary tumor tissue. Combined MPE/SHG clearly demonstrates the ability to image deep into live tissue and obtain meaningful information from endogenous signals. In (b), emission signals were isolated with a 464-nm (cut-on) long-pass filter for MPE (pseudocolored red) and a 445-nm narrow bandpass filter SHG (pseudocolored green). This approach permits identification of epithelial tumor cells, tumor-associated stromal cells, and the collagen matrix. As such, combined MPE/SHG imaging of intact tumors can provide relevant information about the cell-matrix interaction and how matrix density and organization influence cell behavior. Bar = 25 μm.

Fig. 2 FLIM imaging of live mammary tumor tissue. Tumors were imaged at $\lambda_{ex}=780$ nm [(a) and (b)] and $\lambda_{ex}=890$ nm [(c) and (d)] to produce endogenous fluorescence from NADH and FAD, respectively. Intensity [(a) and (c)] and color-mapped lifetime [(b) and (d)] images are shown. Color mapping represents the weighted average of the mean lifetime (τ_m) (Eq. (2)) following fitting with a two-term exponential model [Eq. (1)]. Note that emission from collagen (d) maps to the yellow end of the spectrum, indicating SHG.

as well as signatures that identify invading metastatic cells.[14] TACS-1 characterizes the presence of increased SHG signal intensity due to increased locally dense collagen within the globally increased collagen concentration surrounding tumors, serving as a reliable hallmark for locating small neoplastic regions. TACS-2 classifies straightened collagen fibers stretched around the tumor, constraining the tumor volume and indicating that the tumor has substantially expanded and is straining the space of its microenvironment. TACS-3 is the identification and characterization of radially aligned (distributed at approximately 90 deg relative to the tumor boundary) collagen fibers that facilitate local invasion, and support evidence presented by Condeelis and colleagues that metastasizing tumor cells migrate along collagen fibers.[3,26]

Multiphoton FLIM provides an additional data dimension—allowing the measurement of the fluorescence lifetimes of endogenous fluorophores within normal and tumor cells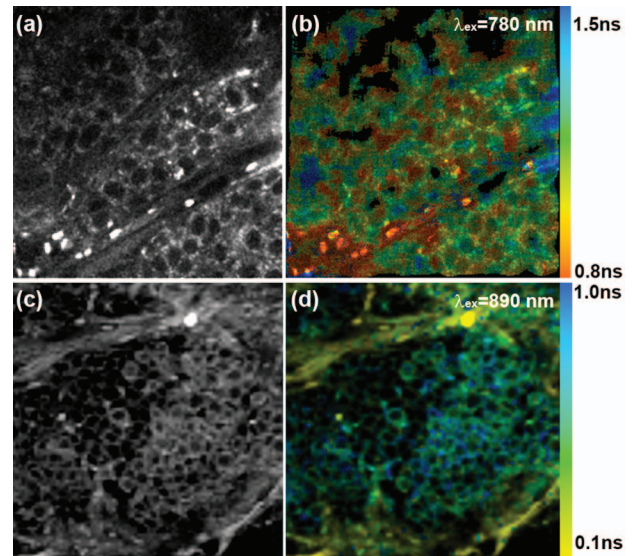 while simultaneously identifying collagen in and around the tumor by exploiting the fact that the collagen signal is not fluorescent and as such has a theoretical lifetime of zero. Figure 2 demonstrates the utility of multiphoton FLIM in identifying and measuring lifetimes of the relevant metabolic components NADH and FAD, as well as identifying collagen. To characterize and present lifetime information, the data was fit with a multiexponential model:

$$I_f(t) = \sum_{i=0}^{n} a_i \exp(-t/\tau_i) + \mathrm{c} = a_1 \exp(-t/\tau_1) + a_2 \exp(-t/\tau_2)$$
$$+ a_3 \exp(-t/\tau_3) + \cdots . + \mathrm{c}, \tag{1}$$

where a is the fractional contribution of each of the compo-
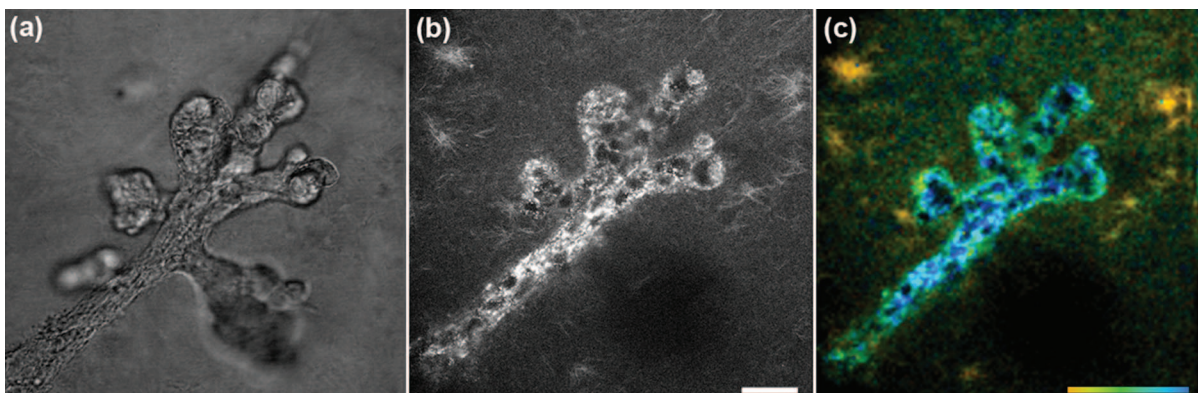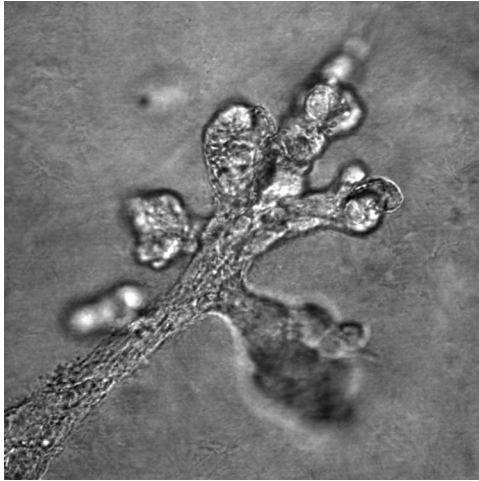

Fig. 3 Imaging mammary ductal structure in reconstituted 3-D matrices. Nontransformed NMuMG mammary cells were cultured within a 3-D collagen matrix (3.0 mg/mL) for 7 days to demonstrate the ability of combined MPE/SHG/FLIM to study cellular differentiation and the extracellular microenvironment. The recapitulated ductal structure can be seen with transmitted light (a), but use of combined MPE/SHG (b) and/or multiphoton FLIM (c) provides information regarding the collagen matrix and the physiologic state of the cells. In (c), color represents the weighted average following a two-term exponential fit as described in Fig. 2. Scale bar=25 μm; color bar 0.08 to 1.0 ns (red to blue).

Video 1. Movie of a transmitted light *z*-stack (200 μm), showing mammary ductal structure with a reconstituted 3-D matrix (Quick-Time, 2.7 MB). [URL: http://dx.doi.org/10.1117/1.2940365.1].

Video 2. Pseudocolored movie of a combined MPE/SHG *z*-stack (200 μm), showing ductal structure and the surrounding collagen microenvironment (QuickTime, 4.49 MB).
[URL: http://dx.doi.org/10.1117/1.2940365.2].

nents, τ is the fluorescence lifetime, and c is background light noise. By examining the relative contributions of the lifetime components as well as their value, it may be possible to identify a particular fluorophore or gain an understanding about biological processes that are influencing a fluorophore. In Fig. 2, the data are presented as a weighted average of a two-component lifetime fit:

$$\tau_m = (a_1\tau_1 + a_2\tau_2)/(a_1 + a_2). \qquad (2)$$

Hence, FLIM can help identify different fluorophores, with the caveat that absolute identification of the source fluorophore is not certain. However, with the addition of spectral information, much stronger conclusions regarding the emission source can be obtained (see the following).

In addition to the ability to image live tissues, studies in more reductionist *in vitro* systems that reconstruct aspects of the cell's microenvironment, such as reconstituted 3-D matrices, can provide valuable information regarding cell phenotype and signaling events. Figure 3 demonstrates the ability of mammary epithelial to recapitulate ductal structure when cultured under the appropriate conditions within a collagen matrix, supporting the concept of this system as a valuable method to study breast epithelia. Although transmitted light [Fig. 3(a); Video 1] provides information regarding the morphology of the cells and allows visualization of the ductal structure, little information can be obtained regarding the cellular interaction with the microenvironment. By exciting signals from endogenous sources, insight into this interaction can be gained. Combining MPE excitation of endogenous fluorophores with SHG imaging, a more complete view of the structure and its interactions can be obtained [Fig. 3(b); Video 2]. Furthermore, multiphoton FLIM can be utilized as described earlier to acquire lifetime data that can identify the metabolic state of the cell or isolate and characterize fluorophores present with and around the cells. This is of even greater utility when the desired goal is to image both exogenous and endogenous signals simultaneously, such as is the case for protein localization (Fig. 4) or FRET experiments within 3-D collagen environments. As seen in Fig. 4, combined MPE/
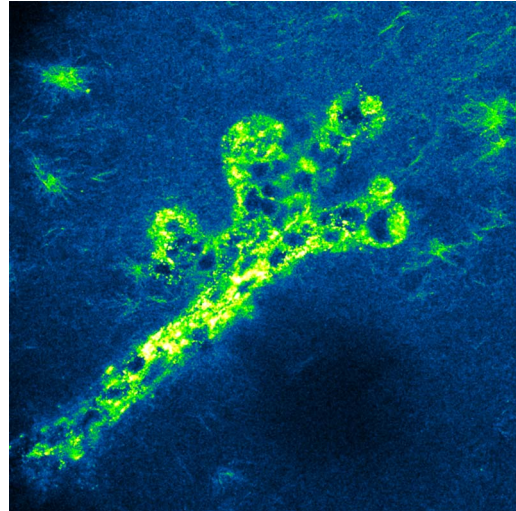
SHG imaging allows a clear view of the cell-matrix interaction in 3-D. GFP emissions from GFP-Vinculin were separated using a 480- to 550-nm (bandpass) filter, while SHG was isolated with a 445-nm narrow bandpass filter. Three-dimensional matrix adhesion to the collagen matrix can clearly be seen (see Fig. 4, inset) allowing a reconstruction of cell morphology, collagen organization, and the cell-matrix interface. However, in more complex studies, such as FLIM, the presence of a strong SHG signal (or other endogenous or exogenous signal) in close proximity to the fluorophore can be very problematic. Moreover, while FRET measured with FLIM can be superior to intensity-based FRET measurements due to the fact that FLIM is independent of fluorophore concentration, FLIM is susceptible to multiple signal contamination issues in data analysis, particularly when more than two lifetime components are potentially present. This can be overcome by employing spectral lifetime imaging, as discussed earlier. By separating the spectral signal of interest from contaminating background[28] or other fluorophores of interest, the lifetime of the fluorophore of interest, can be cleanly obtained (Fig. 5). However, in order to efficiently analyze the large multidimensional data sets from SLIM, a computational infrastructure needs to be developed. As a means to effectively visualize and exploit the information from spectral lifetime data, we have developed a novel computational package.

3.2 *Combined Spectral Lifetime Visualization: SLIM Plotter*

Slim Plotter is a lightweight application for the visualization of combined spectral lifetime data (Fig. 6). The main purpose of the program is to allow exploration of regions of data collected with an SLIM system, but the software also provides some features to assist hardware engineers in proper calibration of the acquisition hardware.

The program is written in Java, which enables cross-platform deployment. Launchers are provided for Microsoft Windows (EXE file), Mac OS X (application bundle), and
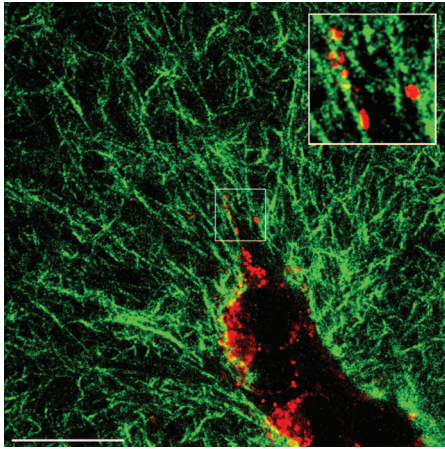
Fig. 4 Imaging 3-D matrix adhesions with MPE/SHG. Combined MPE/SHG imaging at λ_{ex}=890 nm of GFP-Vinculin expressing NMuMG cells within a 3-D collagen matrix (4.0 mg/mL) for 7 days allows a clear view of collagen matrix organization, vinculin localization, and the cell-matrix interaction. Emissions signals from GFP were isolated with a 480 to 550-nm (bandpass) filter (pseudocolored red) and a 445-nm narrow bandpass filter SHG (pseudocolored green). Three-dimensional matrix adhesion to the collagen matrix can clearly be seen (inset). Bar=25 μm.

*nix (shell script). It uses the VisAD Java visualization toolkit for displaying data (http://www.ssec.wisc.edu/~billh/visad.html), which in turn uses Java3D (https://java3d.dev.java.net/). Slim Plotter requires Java version 1.4 and Java3D 1.3—these versions come bundled with Mac OS X, so Slim Plotter should work out of the box on Apple computers, while Windows and Linux users must set up the Java runtime environment and Java3D if they do not already have them installed. Although memory requirements vary depending on the size of the data set, at least 512 MB of system RAM is strongly recommended. See the Slim Plotter website (http://www.loci.wisc.edu/ome/slim.html) for download and detailed installation instructions.

3.2.1 Features

Slim Plotter is designed to be a simple yet effective tool. The main interface fits into one window, with two displays—a 2-D intensity view and a 3-D surface view—plus visualization options and a log window to report numerical results and errors.

3.2.2 Reading data

Slim Plotter uses the LOCI Bio-Formats I/O library (http://www.loci.wisc.edu/ome/formats.html) to read the proprietary
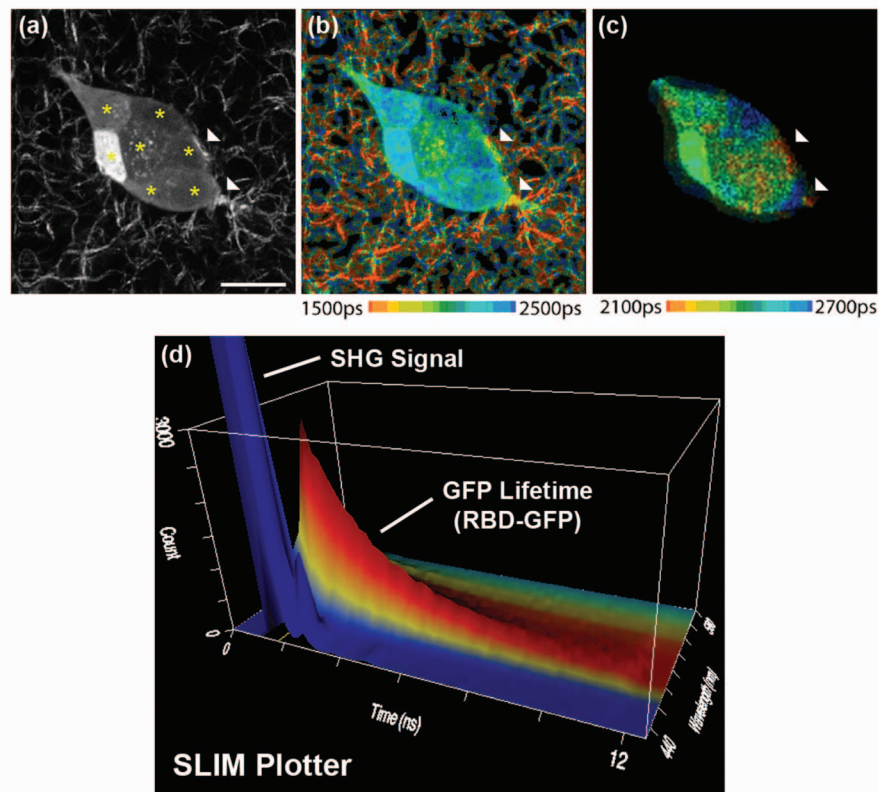

Fig. 5 SLIM to optimize exogenous and endogenous signals. (a) MPE/SHG intensity image of seven T47D breast cells (each designated by a star), composing a developing ductal tubule within a 3-D collagen matrix (1.3 mg/mL) after 5 days in culture. Each cell expresses various levels of EGFP–Rhotekin binding domain (GFP-RBD) and therefore has different intensity in the MPE image. (b) An FLIM image demonstrates collagen fibers in juxtaposition to localized GFP-RBD. Arrows demonstrate regions of localized RBD, suggesting local Rho GTPase activation. Note that Rho is activated at "stress" points where the forming tubule contacts collagen fibers, which is biologically quite interesting but can make data analysis and interpretation difficult. Therefore, the spectral channels for GFP [see the SLIM Plotter output in (d)] were selectively reimaged, producing a new SLIM image, and were color mapped with a narrower lifetime scale (c). This allows elimination of the collagen signal when desired and shows additional localization of GFP-RBD. Hence, spectral lifetime imaging has the ability to facilitate separation of signals of interest for analysis or elimination when the large data set can be efficiently managed and visualized (see Sec. 3.2). Bar=20 μm.
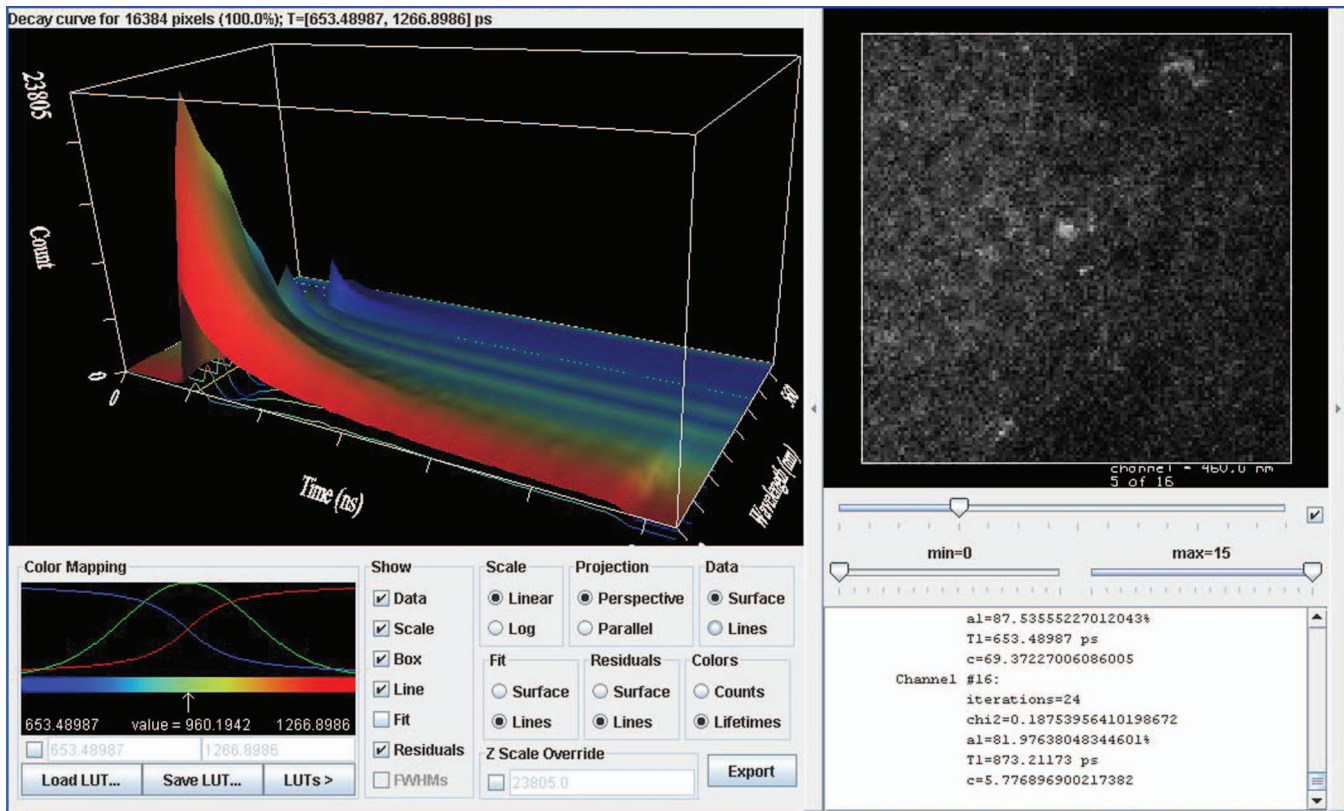
Fig. 6 SLIM Plotter Visualization window. Example of the SLIM Plotter Visualization window. Data used for this example is from a mammary tumor, and the image shown in the 2-D viewer is a single spectral channel.

SDT data files that the Becker & Hickl FLIM acquisition boards utilize. It supports data of any feasible image resolution, with any number of lifetime bins and spectral channels, including single-channel lifetime data. It automatically extracts the data set's dimensionality (image width, image height, lifetime bin granularity, and number of spectral channels) from the SDT file, but allows the user to override these values if they were stored incorrectly within the file. Some values, particularly the physical width of the lifetime histogram in nanoseconds and the physical width of the spectral range in nanometers, are not present in the SDT format, so the software provides an interface for the user to specify these values (time range, starting wavelength, and channel width). Reasonable defaults are provided—our time range is fixed at 12.5 ns, and channel width is typically 10 nm. Since the starting wavelength can vary, however, Slim Plotter looks at the file name—if the user opted to include the starting wavelength as part of the file name (e.g., 783-890-PML16-440nm-240sec-c.sdt is 440 nm), it uses the indicated value; otherwise, it defaults to 400 nm unless the user overrides the value.

3.2.3 Visualization

One challenge of combined spectral lifetime data is that the sheer dimensionality of the data makes it impossible to show the entire raw data set at once in a comprehensible fashion. Slim Plotter addresses this difficulty with a two-pronged approach: a 2-D image view showing an overview of the data,

with the ability to target a specific region of interest (ROI), and a 3-D plot focusing on the targeted region's details (Fig. 6).

The 2-D image view on the right shows an intensity image for each spectral channel (see Fig. 6). Such intensity images are not directly recorded in the SDT files, but Slim Plotter computes them by summing each lifetime histogram to produce a corresponding aggregate intensity value for each pixel. The slider directly beneath the image controls which channel is currently visible in the display, and Slim Plotter begins with the brightest channel selected. The user can control the 2-D view's brightness and contrast using "min" and "max" sliders beneath the channel selector, which control the image's black level and white level, respectively.

The left plot shows a sum of lifetime decay curves (histograms) for each channel (see Fig. 6). The data is rendered as a surface in 3-D, with the x and z axes corresponding to the histogram's excitation time and photon count, respectively, and the y axis varying across wavelength. The program behaves similarly for single-channel lifetime data, but uses a 2-D line plot for the lifetime histogram, rather than a 3-D surface. The limitation of this view is that it shows only one decay curve per channel, with no facility for differentiating between spatial locations (pixels) within the image. To mitigate this issue, the user can select a ROI by dragging the mouse in the 2-D image view, the pixels are summed and the 3-D surface view displays the totals. In this fashion, the investigator can study lifetime and spectral properties within a

specific structure of the sample. The 3-D view initially displays a sum of all pixels. The user can narrow the focus by encircling a region, or even clicking on an individual pixel. The text directly above the 3-D display indicates the number and percentage of pixels currently being summed.

Initially, the height of the surface is scaled to fit the screen. As such, it can sometimes be difficult to study weaker channels when one channel dominates in intensity. Slim Plotter allows toggling of individual channels using the check box next to the slider beneath the right plot. The program smoothes over any deactivated channels in the surface. It is also possible to fix the z-scale range to an absolute value by checking the Z Scale Override check box and changing the value of the adjacent text field. Furthermore, the z axis can be configured to use a log scale rather than the default linear one by clicking the Log radio button in the Scale options.

To ease discrimination between differing intensity values, the 3-D surface is colored according to a lookup table (LUT). The default table ranges from blue at low levels through the color spectrum to red at high levels, but the table can be customized to provide an alternative color scheme. The LUTs button allows selection of a number of preset color tables, including hue, black-to-red, black-to-green, black-to-blue, black-to-magenta, black-to-cyan, black-to-yellow, grayscale (black-to-white), fire/heat, and ice/cold. The user can also opt to adjust the red, green, and blue color component lines manually by drawing with the mouse. Additionally, the current color table can be saved for later retrieval to a file in a simple binary format compatible with the popular ImageJ program (http://rsb.info.nih.gov/ij/). Last, by default, the color table is automatically scaled such that the smallest value in the surface corresponds to the leftmost color in the table, and the largest value matches the rightmost color. However, at times, it is useful to associate particular colors with absolute values; Slim Plotter enables this behavior with the check box inside the color controls and the two text fields corresponding to the minimum and maximum absolute counts.

There are a few additional visualization options, mostly regarding the 3-D surface view. First, instead of a surface, the data can be rendered as a series of line graphs, one per channel, by clicking the Lines radio button in the Data options. Second, instead of the usual perspective display projection, the program can also show a parallel projection mode, which results in structures along each axis neatly aligned for comparison. Third, the visibility of various components within the display can be toggled, including the bounding box, the scale bars, and the data itself, by using the check boxes in the Show options. Last, the layout of the displays can be rearranged using the left and right arrow buttons surrounding the 2-D view section: clicking the left arrow moves the 2-D view to the left side of the window, while clicking the right arrow causes the 2-D view to break away into its own separate window.

3.2.4 Lifetime curve fitting

In practice, it is expected that the lifetime histograms will conform to an exponential decay pattern in the form [i.e., Eq. (1)]:

$$y(t) = \sum_{i=1}^{n} a_i \exp(-t/\tau_i) + c, \qquad (3)$$

where n represents the number of lifetime components, typically between 1 and 3; a is the scaling factor for each component; c is a background correction factor or offset; and τ corresponds to the expected excited state lifetime per component for the region under analysis.

At present, Slim Plotter can fit single-exponential curves to the lifetime data, to determine an approximation of the aggregate lifetime value per channel. It uses the Levenberg-Marquardt least-squares curve fitting algorithm (LMA) with the help of Janne Holopainen's L-M fit package (http://users.utu.fi/jaolho/). To use the curve fitting feature, the Align Peaks option must be checked when the data is first read (see Sec. 3.2.5). The program log located below the 2-D view shows the exact parameter values of each channel's fitted curve as they are computed, and the text above the left plot details the minimum and maximum aggregate lifetime values across all channels.

The curves are shown superimposed as lines over the data surface in 3-D, making it easy to verify their accuracy. The program also allows visualization of the residuals (differences between expected and actual data values) as lines. Similar to the data itself, the visibility of both the fitted curves and the residuals can be toggled individually using their respective check boxes in the Show options. In addition, the fitted data or the residuals can be shown as surfaces rather than lines, using the corresponding Surface radio buttons.

The default colorization of the 3-D surface data corresponds to surface height; however, if Slim Plotter performs curve fitting, the user can click the Lifetime radio button in the Colors options to colorize the surface instead, based on each channel's aggregate lifetime (τ) value, producing a striped result illustrating lifetime differences between channels. The rules described earlier for colorizing the surface based on height apply equally when visualizing color according to lifetime values.

One last option that is occasionally useful to improve the quality of the curve fit result is the Cut 1.5 ns From Fit check box on the initial confirmation screen, enabled by default. This option disregards the last 1.5 ns of histogram data when performing curve fitting, to compensate for the fact that our system sometimes records a sudden drop in photon counts at the tail end of the lifetime histogram—and the tail values are less important to obtain an accurate fit regardless.

3.2.5 Calibration

Ideally, everything would line up perfectly during collection of spectral lifetime data, with an instant system response time, or at least an equivalent system response delay at each channel. In practice, however, system response skew across channels is one of several practical complications that is associated with a functional spectral lifetime acquisition system. Slim Plotter utilizes an algorithm to correct for slight discrepancies in the system response time between channels: at each channel, the software looks for the histogram's highest value—which should correspond to the peak of the lifetime decay curve—and "pushes forward" individual channels until they all line up. In other words, the program pads these channels

with zeroes so that the channels' decay curve peaks coincide with one another. The program log outputs the results of this alignment when the main window first appears. Unchecking the Align Peaks check box on the initial confirmation screen disables this behavior, but Slim Plotter will not perform exponential curve fitting unless it is allowed to align the peaks.

When calibrating a spectral lifetime system, it is useful for the hardware engineer to perform an acquisition with a second harmonic source (as opposed to a fluorescence sample), which has essentially zero lifetime. Any measured lifetime would therefore be the system response. This response function can be used to deconvolve the fluorescence decay curves so as to correct for the effects of the finite instrument response. Slim Plotter is also capable of analyzing these system response files by computing and visualizing the full width at half maximum (FWHM) values for each channel's lifetime histogram. Since this option is mainly useful for analyzing system response, it is off by default, but it can be enabled by checking the Compute FWHMs check box on the initial confirmation screen. If enabled, Slim Plotter shows the FWHMs as green lines in the 3-D surface view, and their visibility can be toggled using the FWHMs checkbox in the Show options.

3.2.6 Data export

The lifetime histograms currently being viewed can be exported for further processing in another program, using the Export button in the 3-D view controls. Slim Plotter writes the data to a text file in a simple comma-separated values (CSV) format, which can be easily imported into any numeric spreadsheet application.

3.2.7 Slim Plotter future directions

There are a number of improvements we are planning to Slim Plotter to provide more effective analysis of combined spectral lifetime data sets:

• **Integrated VisBio environment**. As part of a larger development effort across our Java software, we are creating a standardized infrastructure of modular components for data I/O, metadata handling, visualization, and analysis. We plan to integrate SLIM Plotter further into this infrastructure, allowing it to utilize these modularized components and to be called as a modular application itself from other applications.

• **Multiexponential curve fitting**. Slim Plotter currently fits only single-exponential lifetime curves. We would like to extend this functionality to support two- and three-component fits, since there are often multiple major lifetime components within the sample, and being able to differentiate between them is critical.

• **Channel binning and SDT export**. SPCImage complements Slim Plotter nicely for lifetime analysis, but SPCImage does not include much support for multispectral data. As such, it would be valuable for Slim Plotter to be able to produce output SDT files with multiple channels binned into one, for use with SPCImage's more sophisticated curve fitting routine.

• **Improved file format**. The SDT format has a number of shortcomings—e.g., the inability to embed time range, starting wavelength, and channel width into the file as metadata—and is somewhat proprietary in nature. We are developing an open format for storing spectral lifetime data based on Heirarchical data format (HDF) and using the OME-XML data model,[50] which both our acquisition system itself and Slim Plotter will support via Bio-Formats.

• **Configurability**. Slim Plotter would benefit from greater configurability. For example, certain parameters such as whether to align the lifetime decay curve peaks must be set when Slim Plotter first starts, and the alignment cannot be toggled or configured afterward. Similarly, the lifetime curve fitting routine itself could benefit from a greater number of options, such as SPCImage's ability to "lock down" certain parameters or adjust the optional 1.5-ns cutoff.

• **Lifetime calibration**. The hardware engineer can collect a system response file that represents the instrument's behavior when no excitation is taking place. Slim Plotter should use this file to adjust the lifetime histograms—by subtracting out the response values—to improve the quality of the fits it generates.

• **Spectral calibration**. Similar to how the system response time differs between spectral channels, creating bias, there is an expected intensity distribution across channels that is not always confluent with reality. Slim Plotter should also calibrate for such system bias to improve spectra-related measurements.

• **Emission spectrum**. The emission spectrum consists of all lifetime bins and pixels summed for each channel, plotted in 2-D as a line graph; Slim Plotter should provide an option for this view.

• **Alternate visualization modes**. Slim Plotter would benefit from additional methods of visualizing the data. For example, a "spectral projection" view could consist of linearly mapping each channel into a position along the visible spectrum (similar to hue), colorizing accordingly, and then performing a maximum intensity projection while preserving the colorization. Slim Plotter could also include the ability to colorize the 2-D view according to each pixel's lifetime by computing the lifetime around that pixel to a particular radius; such a computation is expensive but can be very informative.

In conclusion, we find that combined spectral lifetime imaging has great utility for mitigating the traditional complications presented by endogenous fluorescence and allowing the scientist to fully exploit the power of fluorescence microscopy to record and characterize introduced and native fluorophores *in vivo*. This power of SLIM is demonstrated quite effectively in breast cancer, where many of the key players in cancer invasion and progression are intrinsically fluorescent, and tagged fluorescent constructs for many important signaling molecules have been developed. Rather than having to image the endogenous and exogenous fluorescence separately, as often is done, SLIM allows for simultaneous acquisition and effective discrimination. SLIM will be advanced greatly as photon counting techniques improve with the development of faster photon counting electronics, more sensitive multi-anode detectors, and improved analysis software for curve fitting.

References

1. American Cancer Society, "Cancer facts and figures/cancer statistics," at www.cancer.org(2005–2007).

2. V. Ntziachristos and B. Chance, "Probing physiology and molecular function using optical imaging: applications to breast cancer," *Breast Cancer Res. Treat.* **3**(1), 41–46 (2001).

3. M. Sidani, J. Wyckoff, C. Xue, J. E. Segall, and J. Condeelis, "Probing the microenvironment of mammary tumors using multiphoton microscopy," *J. Mammary Gland Biol. Neoplasia* **11**(2), 151–163 (2006).

4. W. R. Zipfel, R. M. Williams, R. Christie, A. Y. Nikitin, B. T. Hyman, and W. W. Webb, "Live tissue intrinsic emission microscopy using multiphoton-excited native fluorescence and second harmonic generation," *Proc. Natl. Acad. Sci. U.S.A.* **100**(12), 7075–7080 (2003).

5. G. Cox, E. Kable, A. Jones, I. Fraser, F. Manconi, and M. D. Gorrell, "Three-dimensional imaging of collagen using second harmonic generation," *J. Struct. Biol.* **141**(1), 53–62 (2003).

6. A. Zoumi, A. Yeh, and B. J. Tromberg, "Imaging cells and extracellular matrix *in vivo* by using second-harmonic generation and two-photon excited fluorescence," *Proc. Natl. Acad. Sci. U.S.A.* **99**(17), 11014–11019 (2002).

7. E. Brown, T. McKee, E. DiTomaso, A. Pluen, B. Seed, Y. Boucher, and R. K. Jain, "Dynamic imaging of collagen and its modulation in tumors *in vivo* using second-harmonic generation," *Nat. Med.* **9**(6), 796–800 (2003).

8. W. Denk, J. H. Strickler, and W. W. Webb, "Two-photon laser scanning fluorescence microscopy," *Science* **248**(4951), 73–76 (1990).

9. W. Wang, S. Goswami, E. Sahai, J. B. Wyckoff, J. E. Segall, and J. S. Condeelis, "Tumor cells caught in the act of invading: their strategy for enhanced cell motility," *Trends Cell Biol.* **15**(3), 138–145 (2005).

10. P. J. Campagnola, A. C. Millard, M. Terasaki, P. E. Hoppe, C. J. Malone, and W. A. Mohler, "Three-dimensional high-resolution second-harmonic generation imaging of endogenous structural proteins in biological tissues," *Biophys. J.* **82**(1, Pt. 1), 493–508 (2002).

11. E. B. Brown, R. B. Campbell, Y. Tsuzuki, L. Xu, P. Carmeliet, D. Fukumura, and R. K. Jain, "*In vivo* measurement of gene expression, angiogenesis and physiological function in tumors using multiphoton laser scanning microscopy," *Nat. Med.* **7**(7), 864–868 (2001).

12. V. E. Centonze and J. G. White, "Multiphoton excitation provides optical sections from deeper within scattering specimens than confocal imaging," *Biophys. J.* **75**(4), 2015–2024 (1998).

13. J. M. Squirrell, D. L. Wokosin, J. G. White, and B. D. Bavister, "Long-term two-photon fluorescence imaging of mammalian embryos without compromising viability," *Nat. Biotechnol.* **17**(8), 763–767 (1999).

14. P. P. Provenzano, K. W. Eliceiri, J. M. Campbell, D. R. Inman, J. G. White, and P. J. Keely, "Collagen reorganization at the tumor-stromal interface facilitates local invasion," *BMC Med.* **4**(1), 38 (2006).

15. S. Ameer-Beg, P. R. Barber, R. J. Hodgkiss, R. J. Locke, R. G. Newman, G. M. Tozer, B. Vojnovic, and J. Wilson, "Application of multiphoton steady state and lifetime imaging to mapping of tumor vascular architecture *in vivo*," *Proc. SPIE* **4620**, 85–95 (2002).

16. K. W. Eliceiri, C. H. Fan, G. E. Lyons, and J. G. White, "Analysis of histology specimens using lifetime multiphoton microscopy," *J. Biomed. Opt.* **8**(3), 376–380 (2003).

17. E. Gratton, S. Breusegem, J. Sutin, Q. Ruan, and N. Barry, "Fluorescence lifetime imaging for the two-photon microscope: time-domain and frequency-domain methods," *J. Biomed. Opt.* **8**(3), 381–390 (2003).

18. T. French, P. T. So, D. J. Weaver, Jr., T. Coelho-Sampaio, E. Gratton, E. W. Voss Jr., and J. Carrero, "Two-photon fluorescence lifetime imaging microscopy of macrophage-mediated antigen processing," *J. Microsc.* **185**(Pt 3), 339–353 (1997).

19. D. K. Bird, K. W. Eliceiri, C. H. Fan, and J. G. White, "Simultaneous two-photon spectral and lifetime fluorescence microscopy," *Appl. Opt.* **43**(27), 5173–5182 (2004).

20. A. Ruck, C. Hulshoff, I. Kinzler, W. Becker, and R. Steiner, "SLIM: a new method for molecular imaging," *Microsc. Res. Tech.* **70**(5), 485–492 (2007).

21. J. Lippincott-Schwartz, E. Snapp, and A. Kenworthy, "Studying protein dynamics in living cells," *Nat. Rev. Mol. Cell Biol.* **2**(6), 444–456 (2001).

22. J. Lippincott-Schwartz and G. H. Patterson, "Development and use of fluorescent protein markers in living cells," *Science* **300**(5616), 87–91 (2003).

23. J. Zhang, R. E. Campbell, A. Y. Ting, and R. Y. Tsien, "Creating new fluorescent probes for cell biology," *Nat. Rev. Mol. Cell Biol.* **3**(12), 906–918 (2002).

24. M. Parsons, J. Monypenny, S. M. Ameer-Beg, T. H. Millard, L. M. Machesky, M. Peter, M. D. Keppler, G. Schiavo, R. Watson, J. Chernoff, D. Zicha, B. Vojnovic, and T. Ng, "Spatially distinct binding of Cdc42 to PAK1 and N-WASP in breast carcinoma cells," *Mol. Cell. Biol.* **25**(5), 1680–1695 (2005).

25. M. Peter, S. M. Ameer-Beg, M. K. Hughes, M. D. Keppler, S. Prag, M. Marsh, B. Vojnovic, and T. Ng, "Multiphoton-FLIM quantification of the EGFP-mRFP1 FRET pair for localization of membrane receptor-kinase interactions," *Biophys. J.* **88**(2), 1224–1237 (2005).

26. W. Wang, J. B. Wyckoff, V. C. Frohlich, Y. Oleynikov, S. Huttelmaier, J. Zavadil, L. Cermak, E. P. Bottinger, R. H. Singer, J. G. White, J. E. Segall, and J. S. Condeelis, "Single cell behavior in metastatic primary mammary tumors correlated with gene expression patterns revealed by molecular profiling," *Cancer Res.* **62**(21), 6278–6288 (2002).

27. W. Wang, S. Goswami, K. Lapidus, A. L. Wells, J. B. Wyckoff, E. Sahai, R. H. Singer, J. E. Segall, and J. S. Condeelis, "Identification and testing of a gene expression signature of invasive carcinoma cells within primary mammary tumors," *Cancer Res.* **64**(23), 8585–8594 (2004).

28. P. P. Provenzano, K. W. Eliceiri, L. Yan, A. Ada-Nguema, M. W. Conklin, D. R. Inman, and P. J. Keely, "Nonlinear optical imaging of cellular processes in breast cancer," *Microsc. Microanal.* (in press).

29. D. K. Bird, L. Yan, K. M. Vrotsos, K. W. Eliceiri, E. M. Vaughan, P. J. Keely, J. G. White, and N. Ramanujam, "Metabolic mapping of MCF10A human breast cells via multiphoton fluorescence lifetime imaging of the coenzyme NADH," *Cancer Res.* **65**(19), 8766–8773 (2005).

30. G. M. Palmer, P. J. Keely, T. M. Breslin, and N. Ramanujam, "Autofluorescence spectroscopy of normal and malignant human breast cell lines," *Photochem. Photobiol.* **78**(5), 462–469 (2003).

31. N. D. Kirkpatrick, C. Zou, M. A. Brewer, W. R. Brands, R. A. Drezek, and U. Utzinger, "Endogenous fluorescence spectroscopy of cell suspensions for chemopreventive drug monitoring," *Photochem. Photobiol.* **81**(1), 125–134 (2005).

32. A. Pradhan, P. Pal, G. Durocher, L. Villeneuve, A. Balassy, F. Babai, L. Gaboury, and L. Blanchard, "Steady state and time-resolved fluorescence properties of metastatic and non-metastatic malignant cells from different species," *Photochem. Photobiol.* **31**(3), 101–112 (1995).

33. R. R. Alfano, A. Pradhan, G. C. Tang, and S. J. Wahl, "Optical spectroscopic diagnosis of cancer and normal breast tissues," *J. Opt. Soc. Am. B* **6**, 1015–1023 (1989).

34. N. Ramanujam, "Fluorescence spectroscopy of neoplastic and non-neoplastic tissues," *Neoplasia* **2**(1–2), 89–117 (2000).

35. R. R. Alfano, B. B. Das, J. Cleary, R. Prudente, and E. J. Celmer, "Light sheds light on cancer—distinguishing malignant tumors from benign tissues and tumors," *Bull. N. Y. Acad. Med.* **67**(2), 143–150 (1991).

36. P. Stoller, B. M. Kim, A. M. Rubenchik, K. M. Reiser, and L. B. Da Silva, "Polarization-dependent optical second-harmonic imaging of a rat-tail tendon," *J. Biomed. Opt.* **7**(2), 205–214 (2002).

37. R. Gauderon, P. B. Lukins, and C. J. Sheppard, "Optimization of second-harmonic generation microscopy," *Micron* **32**(7), 691–700 (2001).

38. R. M. Williams, W. R. Zipfel, and W. W. Webb, "Interpreting second-harmonic generation images of collagen I fibrils," *Biophys. J.* **88**(2), 1377–1386 (2005).

39. J. R. Lakowicz, H. Szmacinski, K. Nowaczyk, K. W. Berndt, and M. Johnson, "Fluorescence lifetime imaging," *Anal. Biochem.* **202**(2), 316–330 (1992).

40. L. Yan, C. T. Rueden, J. G. White, and K. W. Eliceiri, "Applications of combined spectral lifetime microscopy for biology," *BioTechniques* **41**(3), 249, 251, 253 passim (2006).
41. E. Y. Lin, J. G. Jones, P. Li, L. Zhu, K. D. Whitney, W. J. Muller, and J. W. Pollard, "Progression to malignancy in the polyoma middle T oncoprotein mouse breast cancer model provides a reliable model for human diseases," *Am. J. Pathol.* **163**(5), 2113–2126 (2003).
42. D. L. Wokosin, J. M. Squirrell, K. E. Eliceiri, and J. G. White, "An optical workstation with concurrent, independent multiphoton imaging and experimental laser microbeam capabilities," *Rev. Sci. Instrum.* **74**(1), 193–201 (2003).
43. K. W. Eliceiri, personal communication (2006).
44. M. D. Abramoff, P. J. Magelhaes, and S. J. Ram, "Image processing with ImageJ," *Biophotonics Int.* **11**(7), 36–42 (2004).
45. C. Rueden, K. W. Eliceiri, and J. G. White, "VisBio: a computational tool for visualization of multidimensional biological image data," *Traffic (Oxford, U. K.)* **5**(6), 411–417 (2004).
46. L. Ronnov-Jessen, O. W. Petersen, V. E. Koteliansky, and M. J. Bissell, "The origin of the myofibroblasts in breast cancer. Recapitulation of tumor environment in culture unravels diversity and implicates converted fibroblasts and recruited smooth muscle cells," *J. Clin. Invest.* **95**(2), 859–873 (1995).
47. T. D. Tlsty and P. W. Hein, "Know thy neighbor: stromal cells can contribute oncogenic signals," *Curr. Opin. Genet. Dev.* **11**(1), 54–59 (2001).
48. B. Elenbaas, L. Spirio, F. Koerner, M. D. Fleming, D. B. Zimonjic, J. L. Donaher, N. C. Popescu, W. C. Hahn, and R. A. Weinberg, "Human breast cancer cells generated by oncogenic transformation of primary mammary epithelial cells," *Genes Dev.* **15**(1), 50–65 (2001).
49. N. Sato, N. Maehara, and M. Goggins, "Gene expression profiling of tumor-stromal interactions between pancreatic cancer cells and stromal fibroblasts," *Cancer Res.* **64**(19), 6950–6956 (2004).
50. I. G. Goldberg, C. Allan, J. M. Burel, D. Creager, A. Falconi, H. Hochheiser, J. Johnston, J. Mellen, P. K. Sorger, and J. R. Swedlow, "The open microscopy environment (OME) data model and XML file: open tools for informatics and quantitative analysis in biological imaging," *Genome Biol.* **6**(5), R47 (2005).